

Inflow Turbulence Energy and its Spatial Distribution on a Wind Turbine

Christopher Wright

Dr. Lance Manuel

Patrick Ragan

Department of Civil Engineering

Funded by: National Science Foundation, Equal Opportunity in

Engineering, The University of Texas at Austin

Academic Year 2005-2006

Table of Contents

Abstract	1
Introduction	1
Data	2
Project Approach	6
Research Methods	10
Results	13
Conclusions	17
Acknowledgements	17
References	18

Completion report on our project to empirically evaluate energy distribution in unique spatial patterns

Abstract

This study used field data from an instrumented wind turbine, part of Sandia National Laboratories' LIST program, to analyze the spatial distribution of turbulence energy on its rotor plane. Proper Orthogonal Decomposition was performed to evaluate energy distributions from uniform, vertical shear, and lateral shear mode shapes. By binning the data according to wind speeds and different atmospheric parameters, we hoped to minimize the energy distribution among mode shapes within a specific bin, which would aid wind turbine designers in predicting fatigue and extreme loads. The first part of our analysis measured energy distribution within the three mode shapes mentioned previously when binned according to wind speed. Generally, the uniform spatial mode was the most energetic and had the lowest variability in energy, while the vertical shear mode showed greatest variability. The second part of our analysis focused only on the 11-13 (m/s) wind speed bin in which we binned the data based on six atmospheric parameters that were each separated into three equally sized bins. We found that negative atmospheric stability parameters, which indicate an unstable atmosphere, provided the least variability of turbulence energy for the uniform spatial pattern. In the vertical shear mode, high turbulence intensity values caused the most variability of turbulence energy while high wind shear exponents caused the least.

Introduction

The structural response of a wind turbine is known to be heavily influenced by the spatial distribution of turbulence energy across the rotor plane, but the variability of this distribution has not yet been adequately investigated. This study aims to characterize some of the uncertainty associated with this spatial distribution. If there is high uncertainty associated with wind loads on a turbine, it must be conservatively over-designed, and such an approach leads to a higher manufacturing cost, which ultimately affects the price of the power produced.

By obtaining the time-synchronized wind speeds at different locations about the rotor plane of a turbine, the amount of turbulence energy present in specific spatial

patterns can be studied using Proper Orthogonal Decomposition (POD). The appropriate measured (field) data for this type of spatial analysis has been provided by Sandia National Laboratories' Long-Term Inflow and Structural Test (LIST) Program which was conducted on a wind turbine in Bushland, Texas. We studied the influence that various atmospheric parameters have on the variability of energy within these spatial patterns. Specifically, by binning the data according to different parameters, we hoped to find one or more parameters which are associated with reduced uncertainty in the spatial energy distribution. Such parameters could then be used by designers to help predict what moments that structure is likely to experience at a specific site.

Data

The LIST Turbine in Bushland, Texas is one of three modified Micon 65/13M wind turbines that have been erected at the USDA Agriculture Research Service (ARS) center in Bushland, Texas [1,2]. These turbines formerly ran in the Palm Springs (CA) area for approximately 15 years, but many of the subsystems such as the brakes, generator, and blades were modified to increase performance and reliability. Each turbine is a fixed pitch, 3-bladed up-wind turbine with an asynchronous, three-phase 480v generator rated at 115 kW. With a hub height of 23 m, the blades turn at a fixed 55 rpm (10 rpm more than the standard Micon 65/13 turbine) and the generator operates at 1200 rpm. The three turbines were monitored with 59 instruments that collected 1,630 hours of continuous inflow and structural response data [1]. 34 of the instruments were used to characterize the inflow, 18 were for characterizing the structural response, and 7 were used to characterize the time varying state of the turbine. The sensors all have a sampling

frequency of 30 Hz (i.e., they take 30 measurements every second). The data we used was from the second LIST measurement campaign. The initial campaign was terminated due to premature failure of the blade strain gages [1].



Fig 1: LIST Turbine (center), sister turbines, and meteorological towers from which the data was collected in Bushland, TX. (Photo courtesy: Perry L. Jones, Sandia National Laboratories)

The LIST turbine had 7.9 m long Solar Energy Research Institute (SERI) blades with a rotor diameter of 17.1 m and was located in between the two sister turbines [2]. The LIST turbine was the only one equipped with five sonic anemometers on three meteorological towers located 27.98 m southwest of the turbine. The towers were located approximately 1.8 diameters away from the LIST turbine so the wind speed measurements would not be affected by the spinning of the turbine blades. The data recorded from the array of five sonic anemometers was used in this analysis to characterize the inflow into the LIST turbine. The following figures show the LIST turbine and the spatial distribution of sonic anemometers about the rotor.



Fig. 2: The Micon 65/13M Turbine at the Bushland Test Site.

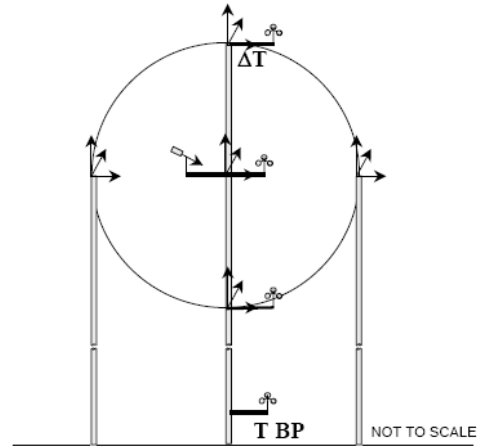


Fig. 3: Schematic Diagram of the Inflow Instrumentation for the LIST Turbine.

Notation:



The wind measurements were recorded as ten-minute time synchronized continuous data streams that initially contained 9,801 recordings [1]. Many of the recordings were not used for the following reasons: they had average wind speeds less than 7 m/s, the anemometers got blocked temporarily, or the turbine wasn't operating during an entire ten-minute segment (2nd campaign paper). After eliminating the bad records, there were 4,609 records remaining, many of which were still damaged due to instrument malfunctions and had to be discarded before we ran our analysis. The following figure shows an example of an undamaged wind speed recording compared to a damaged recording.

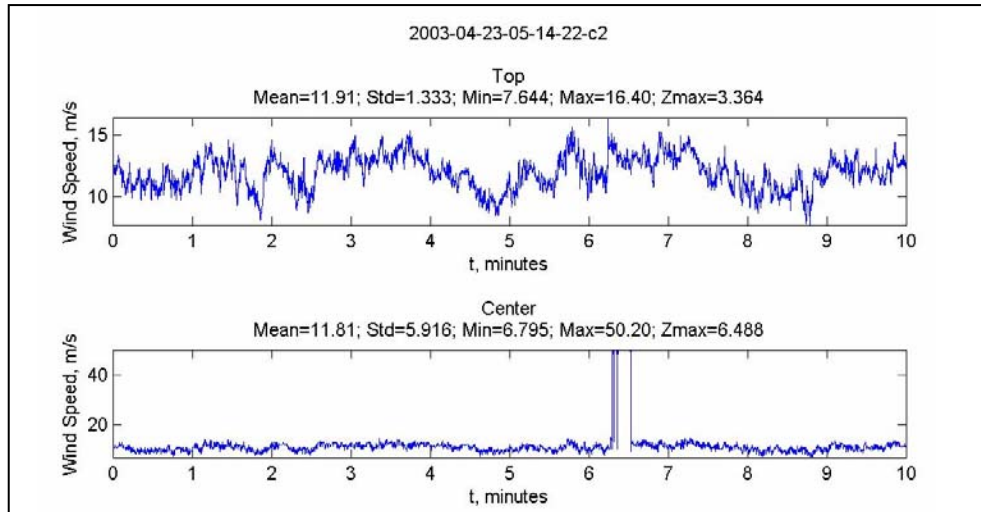


Figure 4: Undamaged wind speed recording (top) and damaged recording (bottom)

894 records (approximately 20% of our initial records) were detected as damaged files and removed from our data set. Each of the 3,715 remaining ten-minute records contained 75 channels of information including wind speeds, atmospheric conditions, and structural responses from the turbine. The following figure shows the distribution of ten-minute records used in our analysis relative to mean wind speed.

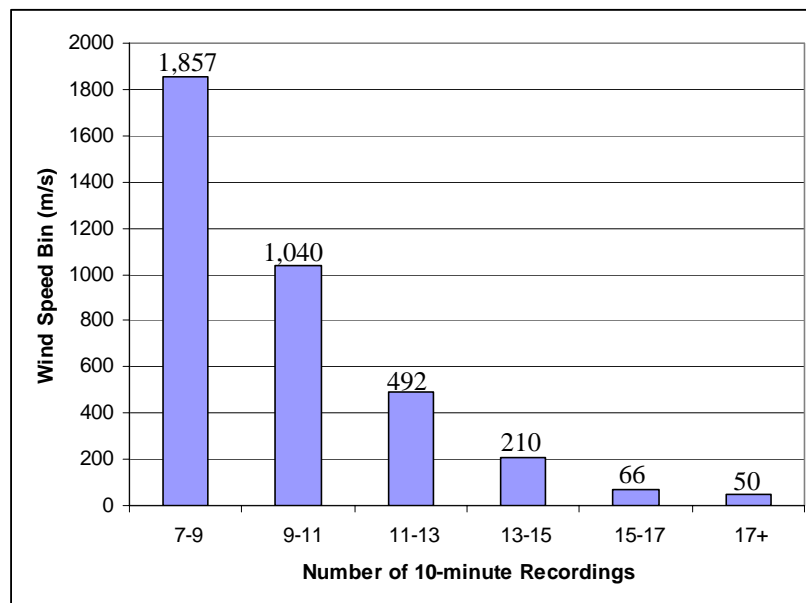


Figure 6: Number of Records in each Wind Speed Bin

Project Approach

Using the MATLAB computer program, programs were written to manipulate the data obtained from the LIST turbine. First we used visual representations of the recorded wind speeds to filter out the damaged records from the usable ones. Next, we performed a Proper Orthogonal Decomposition (POD) analysis on the mean wind speeds in five locations about the rotor.

POD is an empirical technique that can be used to decompose a high dimensional random process into preferred spatial patterns (modes) [3]. These modal shapes are revealed by first creating a covariance matrix, \mathbf{C}_p from the along wind and cross wind measurements of average wind speeds, $\mathbf{P}(t)$ at N locations about the rotor.

$$\mathbf{P}(t) = \{ P_1(t) \quad P_2(t) \quad \dots \quad P_N(t) \}^T \quad (1)$$

$$\mathbf{C}_p = \begin{bmatrix} C_{P_1P_1} & C_{P_1P_2} & \dots & C_{P_1P_N} \\ C_{P_2P_1} & C_{P_2P_2} & \dots & C_{P_2P_N} \\ \vdots & \vdots & \dots & \vdots \\ C_{P_NP_1} & C_{P_NP_2} & \dots & C_{P_NP_N} \end{bmatrix} \quad (2)$$

From this covariance matrix, $\mathbf{P}(t)$ can be projected onto different modes, Φ by decomposing $\mathbf{P}(t)$ into orthogonal vectors with uncorrelated random processes, $\mathbf{a}(t)$ as coefficients.

$$\mathbf{a}(t) = \Phi^T \mathbf{P}(t) \Rightarrow \mathbf{P}(t) = \Phi \mathbf{a}(t) = \sum_{n=1}^N \Phi_n a_n(t) \quad (3)$$

$$\begin{Bmatrix} P_1(t) \\ P_2(t) \\ \vdots \\ P_N(t) \end{Bmatrix} = a_1(t) \begin{Bmatrix} \phi_{11} \\ \phi_{21} \\ \vdots \\ \phi_{N1} \end{Bmatrix} + a_2(t) \begin{Bmatrix} \phi_{12} \\ \phi_{22} \\ \vdots \\ \phi_{N2} \end{Bmatrix} + \dots + a_N(t) \begin{Bmatrix} \phi_{1N} \\ \phi_{2N} \\ \vdots \\ \phi_{NN} \end{Bmatrix} \quad (4)$$

↑ Mode 1 ↑ Mode 2 ↑ Mode N

time ↓

space ↙

C_p can then be transformed into an uncorrelated covariance matrix, Λ from which eigenvalues, λ_n and eigenvectors, Φ_n can be extracted to reveal the turbulence energy and shape for five modes, respectively.

$$C_p \Phi = \Phi \Lambda \Leftrightarrow \Phi^T C_p \Phi = \Lambda \quad (5)$$

$$\Lambda = \begin{bmatrix} \lambda_1 & 0 & \dots & 0 \\ 0 & \lambda_2 & \dots & 0 \\ \vdots & \vdots & \dots & \vdots \\ 0 & 0 & \dots & \lambda_N \end{bmatrix}, \quad \Phi = \begin{bmatrix} \phi_{11} & \phi_{12} & \dots & \phi_{1N} \\ \phi_{21} & \phi_{22} & \dots & \phi_{2N} \\ \vdots & \vdots & \dots & \vdots \\ \phi_{N1} & \phi_{N2} & \dots & \phi_{NN} \end{bmatrix} \quad (6)$$

By plotting the modal coordinates given by the eigenvectors of the uncorrelated covariance matrix Λ , we observed different shapes that characterize how certain percentages of inflow energy were being distributed across the rotor. There were generally five main shapes that were observed and the mode which they belonged to depended upon the eigenvalues, or turbulence energy, present in each particular shape. The mode numbers were initially assigned from one to five according to the magnitude of the eigenvalue. Therefore, the first mode always had the highest percentage of total energy in each recording and the fifth mode always had the least. The following figure shows results of this procedure for a sample ten-minute time series.

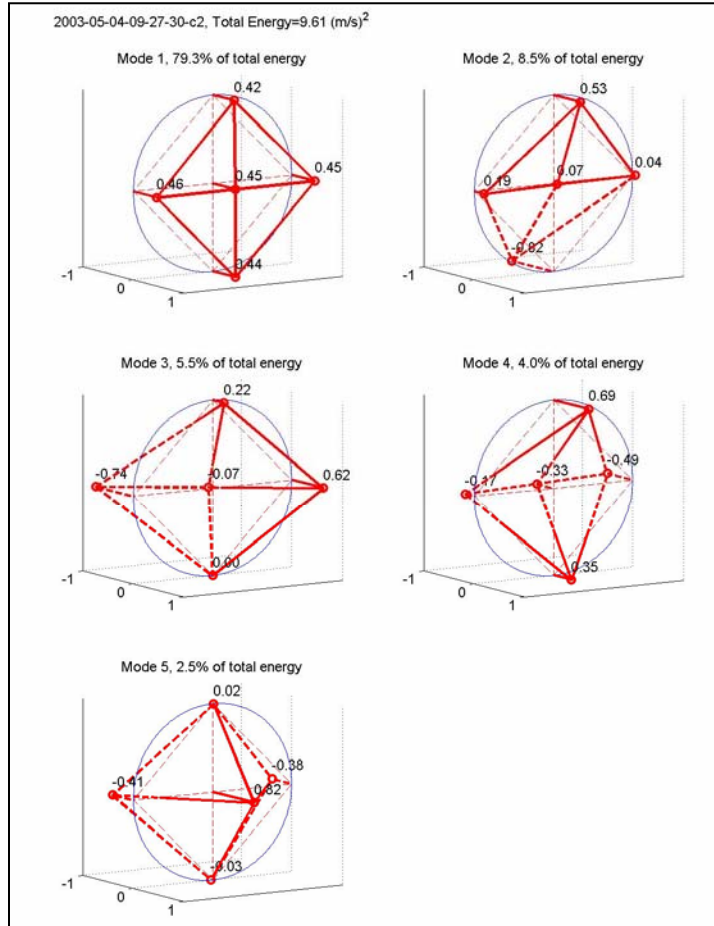


Figure 7: Mode shapes and percentages of total energy

Typically, the first mode had a very large percentage of the total energy in a given ten-minute recording, and it was almost always characterized by a uniform shape across the rotor. The second and third modes varied in shape between vertical shear and lateral shear. Usually the vertical shear shape would have more energy than the lateral shear, but sometimes the lateral shear contained more energy and would therefore be in the second mode instead of the third. Measuring the energy distribution within mode shapes was more quantitative if we identified each mode with a certain shape and observed the variation of energy within that shape than if we had compared the variation in shape with respect to a certain percentage of total energy.

To separate modes by shape rather than energy, we took the dot product of each mode's eigenvectors with the unit vector that would signify an ideal vertical or lateral shear shape. For example, to detect the mode which displayed the shape most similar to vertical shear, we found the dot product of the eigenvectors of each mode with the array: $\left[\frac{1}{\sqrt{2}}, 0, -\frac{1}{\sqrt{2}}, 0, 0 \right]$. This signature vertical shape can be viewed by plotting the previous vectors in the following positions about the rotor: [top, center, bottom, left, right]. It can be seen that the top and bottom coordinates are equal and opposite, while the center, left, and right coordinates are all zero. If the dot product for a particular mode equals one, then that mode shape is identical to the signature vertical shape. Otherwise, we simply define the vertical shape to be the mode whose dot product is closest to one, because then its shape can be considered most similar to the signature shape. The same general procedure was performed to find the shape which most closely resembled lateral shear in each recording. The only difference in the procedure was multiplying the eigenvectors in each mode by the array $\left[0, 0, 0, \frac{1}{\sqrt{2}}, -\frac{1}{\sqrt{2}} \right]$ because this array signifies the ideal lateral shear shape.

The fourth and fifth mode shapes typically made up less than 10% of the total energy for each recording. Because the purpose of our analysis was to aid wind turbine designers in predicting loads that could lead to failure, the amount of energy present in the last two mode shapes was deemed insignificant for our analysis and they were ignored.

Research Methods

Once the first three modes were redefined by shape rather than energy, we measured the energy distribution in each mode shape using the coefficient of variation.

$$\text{COV} = \frac{\sigma}{\mu} \quad (7)$$

where σ is the standard deviation of the turbulence energy present in each mode shape and μ is average amount of turbulence energy present in each mode shape. By comparing the COV of energy distributions for each mode shape, we were able to observe trends relative to different wind speed bins. As the second part of our analysis, we used the same procedure in the 11-13 (m/s) wind speed bin to see if low, medium, or high values of certain inflow parameters would yield low energy distributions within mode shapes.

The following inflow parameters were used for binning in our analysis (where u , v , and w are the along-wind, cross wind, and vertical directions, respectively, and u' , v' , and w' are the corresponding speeds with their means removed) [4]:

- Wind shear exponent, α

$$\frac{U(z_1)}{U(z_2)} = \left[\frac{z_1}{z_2} \right]^\alpha \quad (8)$$

where $U(z_1)$ is the horizontal wind speed at height z_1 . Wind shear exponent is a measure of the increase in horizontal wind speed with height and it is measured by recording wind speeds simultaneously at two points that lie on a vertical line and are separated by a height, z_1 [4]. The three equally sized bins contained the following ranges in wind shear exponents:

Low: Less than 0.085, Medium: 0.085 to 0.115, High: Greater than 0.115

- Stability parameter, z/L

$$z/L \quad (9)$$

where z is the hub height elevation and L is the Obukhov length.

- Obukhov length, L

$$L = \frac{-\bar{\theta}_s (U^*)^3}{0.4g(w'\theta'_s)} \quad (10)$$

where $\bar{\theta}_s$ is the mean hub-height pressure-corrected temperature in °K, g is the acceleration due to gravity (9.81 m/s²), and U^* is the local friction velocity [4].

- Local friction velocity, U^*

$$U^* = \sqrt{u'w'} \quad (11)$$

Stability parameters can be classified into three categories with negative values representing unstable atmospheres, 0 values representing neutral atmospheres, and positive values representing stable atmospheres [5]. The three equally sized bins contained the following ranges in stability parameters:

Low: Less than -0.117, Medium: -0.117 to 0.015, High: Greater than 0.015

- Turbulence Intensity, I

$$I = \frac{\sigma}{\mu} \quad (12)$$

where μ is the average wind speed for a ten-minute recording and σ is the standard deviation of the wind speeds in that recording. The three equally sized bins contained the following ranges in turbulence intensities:

Low: Less than 11.14%, Medium: 11.14% to 13.2%, High: Greater than 13.2%

- Gradient Richardson Number, Ri

$$Ri = \frac{g}{\Theta_m} \left(\frac{\Delta\Theta(z)}{\Delta z} \right)_{ave} \left[\left(\frac{\Delta U(z)}{\Delta z} \right)_{ave} \right]^{-2} \quad (13)$$

where Θ_m is the mean virtual potential temperature in °K between the top and

bottom of the tower, $\left(\frac{\Delta\Theta(z)}{\Delta z} \right)_{ave}$ is the average vertical gradient of the virtual

potential temperature using all temperature measurements, and $\left(\frac{\Delta U(z)}{\Delta z} \right)_{ave}$ is the

average vertical gradient of the wind speed using all wind speed measurements.

A Richardson Number greater than 0.01 means that the atmosphere is stable [4].

The three equally sized bins contained the following ranges in Richardson

Numbers:

Low: Less than 0.0027, Medium: 0.0027 to 0.155, High: Greater than 0.155

- Along-Wind Turbulence Length Scale, L_u

$$L_u = \bar{U}_s \int_0^T R_u(\tau) d\tau \quad (14)$$

where \bar{U}_s is the mean wind speed in the along-wind direction, $R_u(\tau)$ is the corresponding autocorrelation function for a lag time, τ , and T is the duration of the record. Along-wind turbulence length scale is a measurement of the maximum distance over which along-wind wind speeds are well correlated [4].

The three equally sized bins contained the following ranges in length scales:

Low: Less than 62 m, Medium: 62 m to 100 m, High: Greater than 100 m

- Wind direction

The primary inflow direction for the LIST turbine in Bushland, TX was 215 ° [2].

The three equally sized bins contained the following ranges in wind directions:

Low: Less than 161°, Medium: 161° to 244°, High: Greater than 244°

Results

It is important to note that in the first part of our analysis, as seen in Figure 4, there were significantly fewer recordings in the higher wind speed bins than in the lower ones. Therefore, the higher wind speed bins have a greater uncertainty when measuring energy distributions simply because there was not as much data as in the lower wind speed bins. The following figure shows the distribution of average total energies relative to the different wind speed bins.

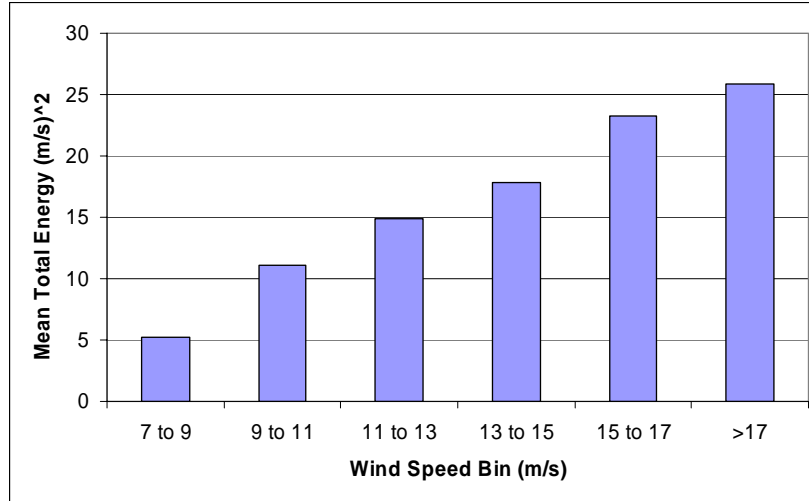


Figure 8: Average total energies in each wind speed bin

It can be seen in the above figure that the average amount of turbulence energy present in each wind speed bin increases almost linearly with increasing wind speed bins. The following figure shows the coefficients of variation from the energy distributions within each mode relative to wind speed bins.

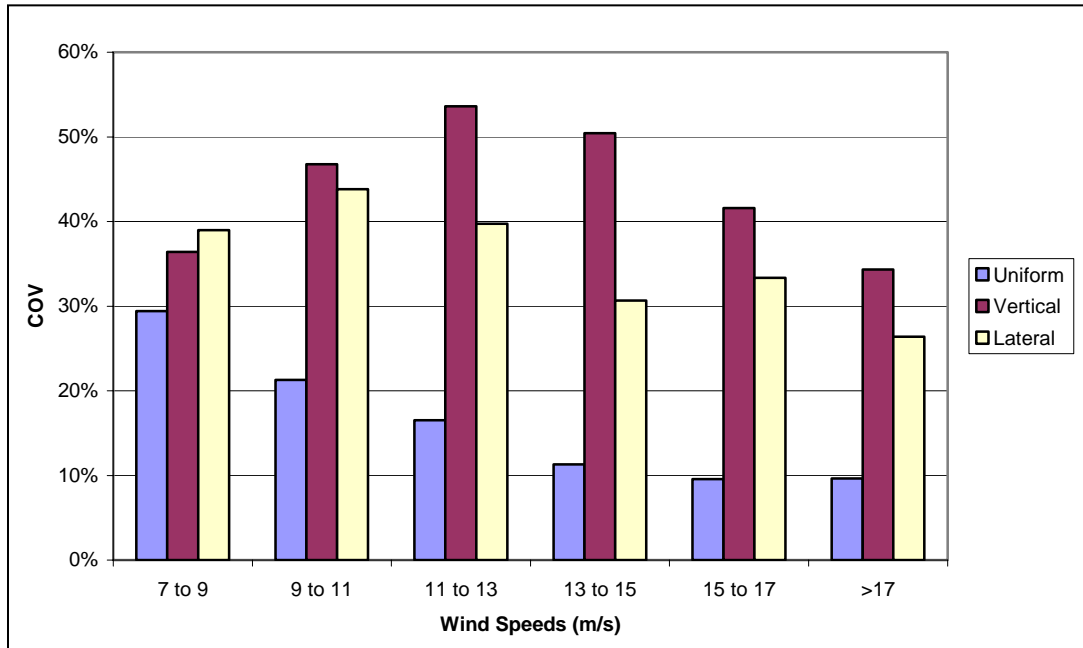


Figure 9: Energy coefficients of variation for three mode shapes in different wind speed bins

It can be seen in the above figure that the COV values of energy distributions in the uniform mode decrease with increasing wind speed bins whereas the COV values

from the vertical and lateral shear mode shapes fluctuate. Furthermore, the 7-9 (m/s) wind speed bin is the only bin in which the energy present in the lateral shear mode shapes were more inconsistent than in the vertical shear mode shapes. From observing Figure 7, it can be concluded that the energy present in the uniform mode shape is more consistent with higher wind speeds than with lower wind speeds.

The following figure shows the distribution of turbulence energy percentages in each mode relative to wind speed bins.

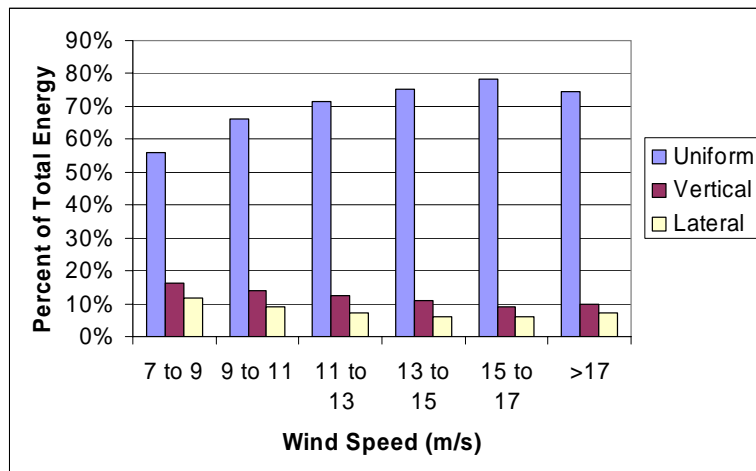


Figure 10: Average mode energy percentages

Figure 8 shows that on average, a much higher percentage of turbulence energy is present in the uniform mode shape than in the vertical and lateral shear modes. It can also be seen that the percentage of energy in the uniform mode generally increases with increasing wind speed. The remaining figure is from the second part of our analysis in which we observed the effects of different atmospheric parameters on energy distributions for different mode shapes within the 11-13 (m/s) wind speed bin. The figure below shows coefficients of variation for energy percentages within modes relative to the six atmospheric parameters discussed in the “Research Methods” section of this report.

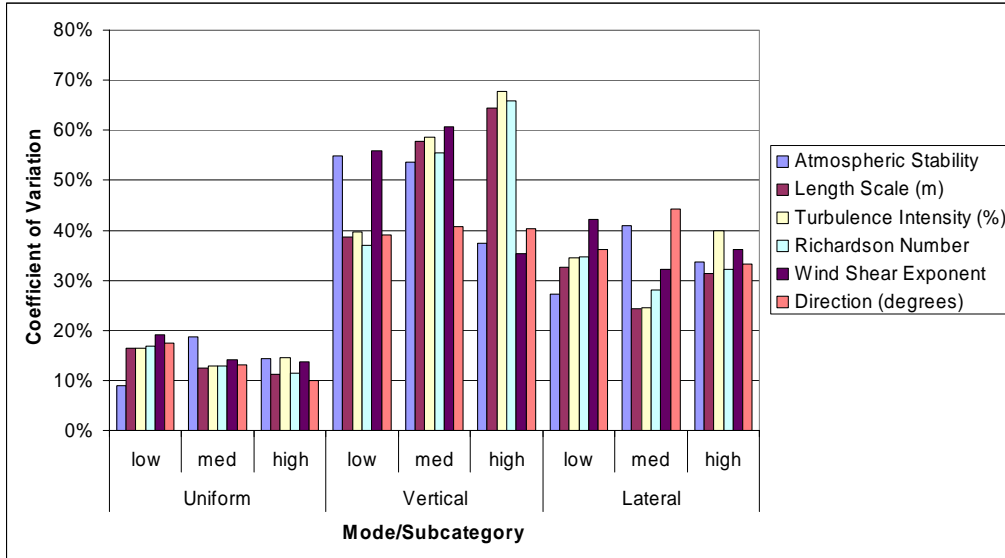


Figure 11: Coefficients of variation for specific parameters within 11-13 m/s wind speed bin

The low, medium, and high values for each parameter can be found in the “Research Methods” section of this report. Once again, it can be seen that the uniform mode had the lowest coefficients of variation in energy. Furthermore, the low atmospheric stability bin had the most consistent eigenvalues in the uniform mode. Because the low atmospheric stability bin consisted of all negative values, it is possible that an unstable atmosphere provides the least energy dispersion for uniform modes within the 11-13 (m/s) wind speed bin. Unstable atmospheres are also the best conditions for power generation because they usually produce high wind speeds [5]. When referring back to the general trend in figure 7, the fact that unstable atmospheres are associated with high wind speeds could be one of the reasons why the energy distribution within the uniform mode shape is so small.

Moreover, Figure 9 shows that within the vertical shear mode, high values of wind shear exponents provided the lowest energy dispersions while high values of turbulence intensity caused the most energy dispersion. It should be noted that many of

these parameters depend on similar variables and therefore trends that take place among certain parameters could be due to those relationships.

Conclusions

Inflow Data from an instrumented wind turbine, part of Sandia's LIST program was analyzed using Proper Orthogonal Decomposition in order to evaluate energy distribution in different spatial patterns empirically. Variability in energy in the first three spatial modes was studied by binning data on the basis of wind speed as well as various other inflow parameters. Generally, the uniform spatial mode was the most energetic and had the lowest variability in energy, while the vertical shear mode showed greatest variability. Atmospheric stability may be a significant parameter in determining the range of energies that the uniform mode will have and a high wind shear exponent could aid designers in accurately predicting the amount of energy that will be present in the vertical shear mode. Among the general mode shapes, there was not a significant variability in modal coordinates in either part of this study.

Acknowledgements

I would like to thank the Texas Research EXperience (TREX) Program for allowing me this opportunity to participate in undergraduate research. Thank you Sandia National Laboratories Contract No. 30914 for providing the data that made this study possible. The National Science Foundation CAREER Grant No. CMS-0449128 deserves much gratitude for making it possible for Patrick Ragan to participate in this study.

References

1. H. Sutherland, J. Zayas, A. Sterns, and B. Neal, "Update of the Long-Term Inflow and Structural Test Program," ASME/AIAA Wind Energy Symposium, Jan. 2004, pp. 1-3
2. Jones, P.L., H.J. Sutherland, and B.A. Neal, LIST/BMI Turbines, Instrumentation and Infrastructure, SAND2001-1642, Sandia National Laboratories, Albuquerque, NM, June 2001, pp. 10-20
3. K. Saranyasoontorn and L. Manuel, "Low-Dimensional Representations of Inflow Turbulence and Wind Turbine Response using Proper Orthogonal Decomposition," Journal of Solar Energy Engineering, Transactions of the ASME, Vol. 127, No. 4, pp. 553-562, November 2005.
4. Nelson, Luke D., "Analysis of Wind Turbine Loads using Inflow and Structural Response Data from Field Measurements," MS Thesis, University of Texas at Austin, May 2003.
5. Rohatgi, Janardan, and Vaughn Nelson. Wind Characteristics: An Analysis for the Generation of Wind Power. Canyon, Texas: Burgess, 1994. pp.36-46